Bispiral approach for calculation of powder spectra of electron paramagnetic and nuclear magnetic resonance

Valentin G. Grachev (valentin.g.grachev@gmail.com)

Research Article

Keywords: powder, spiral, partition, distribution, points on a sphere, electron paramagnetic resonance, nuclear magnetic resonance

Posted Date: March 11th, 2022

DOI: https://doi.org/10.21203/rs.3.rs-1419841/v1

Bispiral approach for calculation of powder spectra of electron paramagnetic and nuclear magnetic resonance

Valentin G. Grachev

SimuMag, 6030 Sir George Lane, Bozeman, Montana 59718, USA

valentin.g.grachev@gmail.com

Simulation of powder spectra uses a summation of spectra calculated for N reference directions of external magnetic field. Usually, the directions are regularly or randomly distributed points on a sphere. Due to an excessive number of points with the same polar angle θ but with different azimuthal angles φ, axial distributions produce jugged spectra, especially for spin systems with weak azimuthal anisotropy. To improve quality of obtained spectra, a triangulation and subsequent interpolation of resonance fields/frequencies for hundred additional directions between triangle vertices or average over a range of magnetic fields/frequencies (tent) are applied. Single spiral method with graduate steps on both θ and φ angles works better for systems with weak azimuthal anisotropy, but allows only few interpolation points along the spiral. Proposed bispiral approach combines best features of both spiral and triangular approaches: exact calculation for N reference spiral directions, joining neighbor points of two spirals into a triangular net, and interpolation over hundred directions or the tent average. For systems with C_1 symmetry the angular space between primary and complementary spirals is exactly equal to the phase space of magnetic fields (hemisphere). For systems with higher symmetry, the angular space can be significantly reduced by a choice of the φ-shift for the second spiral, on a par with the space reduction for axial distributions. The bispiral approach with interpolation over triangles offers manyfold reduction of the calculation time for large spin or multi-spin systems with high ranks of spin-Hamiltonians in comparison with the single spiral grid.

Keywords: powder, spiral, partition, distribution, points on a sphere, electron paramagnetic resonance, nuclear magnetic resonance.

1. Introduction

Recent achievements in nanotechnology and its applications enhance interest in investigations of completely or partly disordered systems by various methods including electron paramagnetic resonance (EPR) and nuclear magnetic resonance (NMR). Simulation of a powder sample spectrum supposes an integration of the magnetic resonance spectrum, calculated at the definite orientation of magnetic field **B** relative to (nano)crystal coordinate axes, over a unit hemisphere of possible orientations of the axial vector **B** [1, 2, 3, 4, 5, 6, 7, 8, 9, 10]. Because in most cases an analytical integration is impossible, the integration is usually substituted by summation over a discrete grid of points on the hemisphere, silently assuming that areas around these points are approximately similar. Below, we consider examples for EPR spectra; however, the basic idea is directly applicable to NMR and other resonance spectra in powders.

A powder spectrum for a single EPR transition can be approximated as follows [4, 8, 9, 11, 12]:

$$S(B) \approx \sum_{k=1}^{N} w_k \, I_k(\theta_k, \varphi_k) F[B - B_0(\theta_k, \varphi_k), W_k(\theta_k, \varphi_k)], \qquad (1)$$

where θ and φ are polar azimuthal angles, I_k is the spectral intensity at the orientation θ_k, φ_k; B_0 is the resonance magnetic field, and $F[B - B_0(\theta_k, \varphi_k), W_k(\theta_k, \varphi_k)]$ is the lineshape absorption function of width W_k. The weighting factors w_k are used to correct non-homogeneity of point distributions on a sphere or boundary conditions for some partitions.

Various regular, semi-regular and random distributions of points on a sphere (partition schemes) were proposed and tested (see [8, 10, 12, 13] for details). Conditionally, we can divide most of the distributions into three categories:

- Axial symmetry (D_{4h} or higher) distributions - simple rectangular grid with equal steps on θ and φ angles (Simfonia [14]), grids with variable steps on φ for equidistant values θ (Igloo [15], SOPHE [16], Easy Spin [17, 18]), octahedral Lebedev grid [19, 20], octahedron based triangulation scheme [21], polar centered grid [22], partitions based on icosahedron [23] or fullerene, etc.
- Random or C_1 symmetry distributions [24], including Monte-Carlo [25, 26], spherical centroidal Voronoi tessellation [27], repulsion [28], Sobol'-Antonov-Saleev [29, 30].
- Spiral and multi-spiral distributions [8, 24, 31, 32, 33], Igloo with rectangular bricks, Fibonacci [34, 35, 36, 37] and Archimedean spirals [38].

We shall denote spectra calculated for these distributions by letters A, R, and S, correspondingly. In principle, using any distribution of points on a sphere gives the same spectrum at a very large density of used points

$$d = \frac{N}{A_S}. \qquad (2)$$

The A_S is the summation area, i.e. the area of the used $\theta\varphi$ space. For the hemisphere of unit radius, the area is equal to 2π, and $d = d_h \equiv N/2\pi$. We shall denote the spectrum calculated for d>10^6 as an ideal, I.

The quality of calculated spectra for different distributions at moderate d and calculation time needed to obtain acceptable smooth spectra are very different (up to several times). Since determination of spectral characteristics requires simulation of dozens, hundreds, or even thousands spectra, the distribution scheme that leads to a shorter calculation time (or to a smoother spectra) is preferable one.

An efficiency of different distributions was analyzed in detail [8, 9, 12, 13]. The spiral and open Sin (Igloo) grids have shown the highest efficiency among 23 tested distributions [8]. The spiral and random (Monte-Carlo) distributions have some advantages in comparison to other grids for N≈580 and W=3 mT [12]. Therefore, below only three grids (Igloo, random, and spiral) are considered (Fig. 1). For all of them, the weights w_k are equal to 1 for all k.

For a comparison of different distribution schemes, let's consider a simple paramagnetic system (or a center) with the spin 1/2, anisotropic **g**-tensor and Gaussian lineshape F_G with an isotropic linewidth W defined as peak-to peak distance of its first derivative

$$F_G = \frac{1}{W\sqrt{2\pi}} \exp\left(-\frac{(B-B_0)^2}{2W^2}\right). \qquad (3)$$

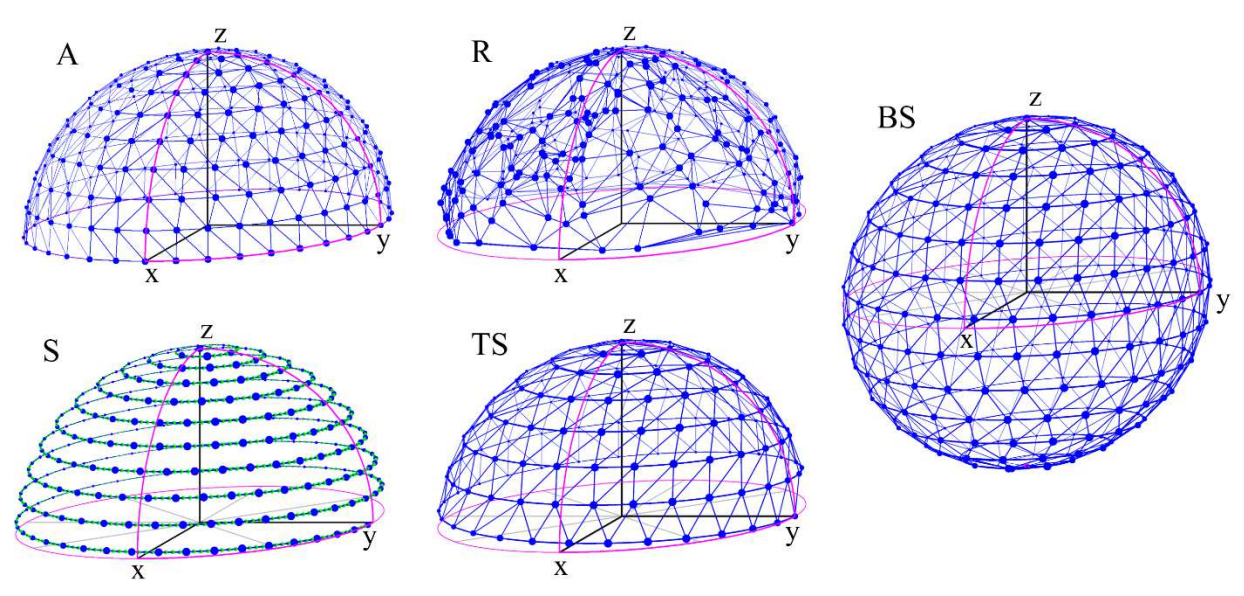

Figure 1. (**Color online**) Point distributions for some representative members of three categories: A –Igloo, R – random, S and TS – single spiral and triangulated spiral on a hemisphere, BS - triangulated full spiral on a sphere.

The minimal number N that gives smooth spectra depends on the average linewidth W for a single crystal spectrum and the spectral extent $\Delta B = B_{finish} - B_{start}$ [31] (or $\Delta\nu$ in the case of NMR). Neighbor lines for different directions of **B** partly overlap if $N >> \Delta B/W$. Simulated spectra of the center for two cases of principal values of g-tensor are presented on Figs. 2 and 3: g_{xx}=2.0, g_{yy}=2.1, g_{zz}=2.2, (the case *a*), and g_{xx}=2.0, g_{yy}=2.0001, g_{zz}=2.2, (the case *b*), for W=0.2 mT. As ΔB≈40mT and N>>200, rather large values of N (about 21185) were used for calculations. This N value corresponds to angular steps $\Delta\theta$=1° for Igloo, SOPHE or Easy Spin distributions, and smaller steps $\Delta\theta \sim \pi/N$ for spiral distribution.

Numerically calculated spectrum is usually represented as a set of intensities $S[m]$, $m = 1, 2, \ldots, M$, where M is the spectrum resolution. To assess the accuracy of simulated spectra two similar (but different) characteristics D [8] and ε [9] were proposed

$$D = \sqrt{\frac{1}{M}\sum_{m=1}^{M}\left[\frac{S_N[m]}{S_I[m]} - 1\right]^2}, \quad (4)$$

$$\varepsilon = 100\sqrt{\sum_{m=1}^{M}(S_N[m] - S_I[m])^2}. \quad (5)$$

Here $S_N[m]$ and $S_I[m]$ are the values of intensities for a spectrum calculated with N angular directions and for an ideal (reference) spectrum. According to [9], the spectra in Eq. (5) must be normalized in the sense

$$\sum_{m=1}^{M} S_N[m] = \sum_{m=1}^{M} S_I[m] = 1. \quad (6)$$

These figures of merit as well as the mean square root deviation (MSRD) have some shortcomings. Very small values of $S_I[m]$ can give relatively large contributions to the D. For instance, a difference between $S_N[m]$~10^{-3} and $S_I[m]$~10^{-5} at several points is unresolved by naked eye but can give contributions that exceed contributions from hundred points near maxima of the spectra. The ε and MSRD overweighs the differences in the more intense parts of the spectrum. For lack of a better merit for singular spectra comparison we shall use the ε below. The ε depends on the used point distribution and density d: the larger the d, the smaller is the ε.

Our simulations (Figs. 2 and 3) show that all spectra are jugged even for such large N values. Spectra for axial and spiral distributions have similar deviations from ideal spectrum for the case (a), whereas for the case (b) the spiral and random distributions give spectra, which are significantly closer to the ideal one than the spectrum for an axial partition. The spiral distribution is an obvious winner for axial or nearly axial centers due to significantly smaller steps on θ: $\Delta\theta \sim \pi/N$ instead of $\Delta\theta \sim \pi/(2\sqrt{2N})$ for axial distributions (Fig. 3).

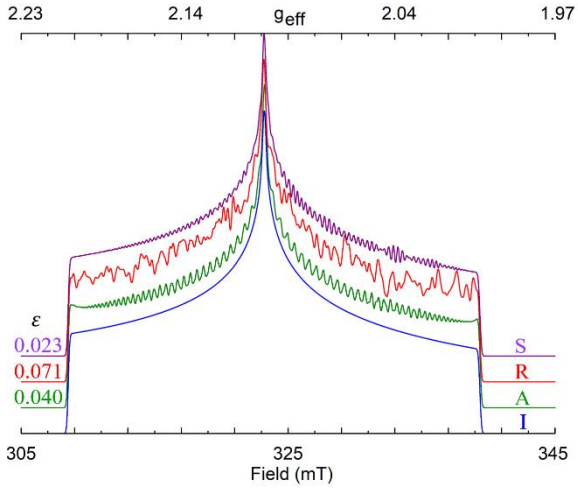

Figure 2. (**Color online**) Simulated spectra for Igloo (A, N=21184), random (R) and spiral (S) distributions (N=21185); g_{xx}=2.0, g_{yy}=2.1, g_{zz}=2.2, W=0.2 mT. I is the ideal spectrum.

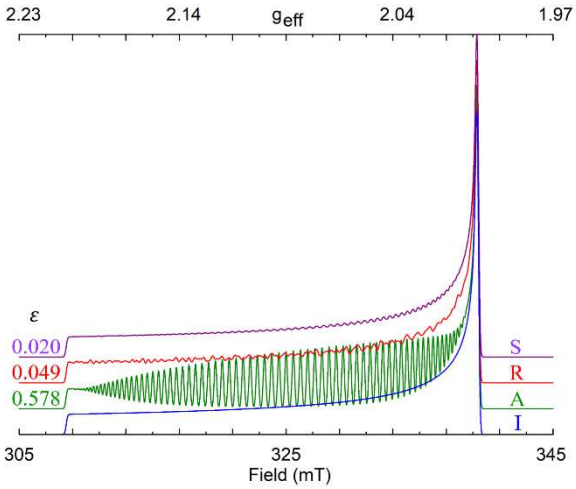

Figure 3. (**Color online**) Simulated spectra for Igloo (A, N=21184), random (R) and spiral (S) distributions (N=21185); g_{xx}=2.0, g_{yy}=2.0001, g_{zz}=2.2, W=0.2 mT. I is the ideal spectrum.

To understand the visible failure of axial distributions in the case b, it is convenient to introduce irreducible components of **g**-tensor:

$$g_{00} = \frac{g_{xx}+g_{yy}+g_{zz}}{3},\ g_{20} = \frac{2g_{zz}-g_{xx}-g_{yy}}{6},\ g_{22} = \frac{g_{xx}-g_{yy}}{2}. \qquad (7)$$

The g_{00} is responsible for the isotropic contribution to spectra, g_{20} describes a polar anisotropy of crystal spectra, and g_{22} – their azimuthal anisotropy. It is easy to find that in the case (a) the absolute values of g_{20}=0.05 and g_{22}=-0.05 are comparable. This leads to a more or less efficient average over all points for all distributions. In the case (b), g_{20}=0.06665 is much larger than g_{22}=-0.00005. Many points with the same θ angle but with different φ angles create a layer in an axial distribution. The layers give separate peaks producing a jugged spectrum. The peaks are very sharp for axial centers with g_{22}=0. However, they are slightly broadened for centers with non-zero values of g_{22}.

There are two basic ideas for spectrum smoothing:

- To insert additional fields/frequencies between three reference fields corresponding to vertices of a triangle (tent, [39, 21]). The number of interpolated fields increases with spectrum resolution.
- To insert N_i additional points in the distributions (sub-partition) and interpolate resonance fields/frequencies for corresponding directions, i.e. to increase density d to about N_i times. 40-150 additional directions N_i are usually sufficient for an effective average over small triangles.

Both smoothing procedures significantly improves spectrum quality, decreasing D and ε more than one order of magnitude. The application of these procedures for axial distributions is

able to give smooth spectra in the case of $g_{20} \approx g_{22}$. For centers with $g_{20} >> g_{22}$ (Fig. 3), the sub-partitioning reduces heights of big teeth in spectra, creating $\sqrt{2N_i}$ peaks of smaller heights.

Points of any distributions can be connected by Delaunay triangulation; however, at large N it consumes a lot of time, decreasing simulation efficiency. Axial distributions allow fast triangulation joining neighbor points.

For a single spiral distribution with the number of spiral points N_s the following interpolation procedure was proposed [31]: to find semi-spiral points with $\Delta\theta = \pi/N_s$, to calculate spectra for every fifth reference spiral direction, and to obtain resonance fields/frequency for N_i intermediate directions (green dots on the spiral on Fig. 1, S) by an interpolation. For larger N_i the angular distance between reference directions increases ($\Delta\theta = \pi N_i/N_s$ and $\varphi = N_i/\sqrt{\pi N_s}$), and the interpolation becomes less accurate, i.e. N_i should be about 4÷6. As the total number of summation points increases from $N_s/(N_i + 1)$ to N_s, the spectra for centers with $g_{20} >> g_{22}$ become smoother. The one-dimensional interpolation is an average along spiral line.

Two-dimensional interpolation schemes with the average over triangles of the triangulated spiral look more efficient; however, a triangulated semi-spiral does not cover the hemisphere due to gaps between the spiral and equator (Fig. 1, TS). Triangulated full spirals are free of gaps and should be used for interpolations (Fig. 1, BS).

Another idea to increase the density d and to improve spectrum quality is to decrease the summation area A_S using symmetry of spin systems. For instance, for centers with C_4 or C_{2v} symmetry the average over the sector restricted by red lines in Fig. 1 gives the same normalized spectrum as the average over hemisphere (see Section 5 for details). The four-time decrease of the area $A_S$allows obtaining four times larger density d for the same N. Such a simple sector reduction of A_S can be easily implemented for most axial distributions (Fig. 1, A), but it is not applicable to random and spiral distributions as they are not compatible with C_4 or C_{2v} symmetry.

In this paper, combining best features of several methods, a significant improvement of the spectrum simulation based on the spiral distribution is proposed. The approach uses two spirals of a multi-spiral family. Both spirals have the same small steps $\Delta\theta$. The neighbor points on two spirals can be quickly joined into a triangular net. The triangulation allows interpolation using both considered smoothing procedures. For spin systems with C_n or higher symmetry, an additional symmetry of the n-spiral family allows 2-12 time reduction of the summation area and a significant increase of spectrum quality.

2. Spiral points on a sphere

To start a spiral on the North Pole and run it to the South Pole the N_s equidistant points on z-axis are introduced by

$$z_k = 1 - \frac{2(k-1)}{N_s - 1}, \quad k=1,\ldots, N_s \tag{8}$$

$$\delta z = z_k - z_{k-1} = \frac{2}{N_s - 1}. \quad (9)$$

Values of angles θ_k and φ_k describing the single spiral are defined precisely by the elliptic integrals of the second kind [40]. However, for powder calculations, the typical values of the N_s are about 500-10,000, i.e. $d\varphi/d\theta \approx \sqrt{\pi N_s} \gg 1$. In this case, there is a simple solution [41, 42, 43]

$$\theta_k = \arccos z_k, \ \varphi_k = c_{N_s}\theta_k. \quad (10)$$

The spiral turn is equal to $\delta\theta = 2\pi/c_{N_s}$ and the distance between two adjacent points is

$$\delta\varphi_k = \varphi_k - \varphi_{k-1} = c_{N_s}\left(\arccos z_k - \arccos(z_k - \delta z)\right) \approx \frac{2c_{N_s}}{N_s\sqrt{1-z_k^2}}. \quad (11)$$

In the equatorial area (that gives dominant contribution to powder spectra), the z_k<<1 and $\delta\varphi_k \approx 2c_{N_s}/N_s$ does not depend on k. For homogeneity of the grid, $\delta\theta$ should be equal to $\delta\varphi$. It gives

$$c_{N_s} = \sqrt{\pi N_s}, \quad (12)$$

and

$$\delta\varphi_k = 2\sqrt{\frac{\pi}{N_s}}\frac{1}{\sqrt{1-z_k^2}}. \quad (13)$$

The coefficient $2\sqrt{\frac{\pi}{N_s}}$ is close to $\frac{3.6}{\sqrt{N_s}}$, which was proposed in [44].

To obtain a homogeneous distribution of points on a sphere for n spirals, which are shifted by $d\varphi_n^{(q)} = 2\pi q/n$, $q = 0,1,..,n-1$, the distance between two adjacent spirals is reduced to $\delta\theta^{(n)} = 2\pi/(nc_{N_S}^{(n)})$, and the value of $c_{N_s}^{(n)}$, which defines the distance $\delta\varphi_k^{(n)}$, is also reduced to

$$c_{N_S}^{(n)} = \sqrt{\frac{\pi N_s}{n}} \quad (14)$$

Finally, the points of the q-th spiral of n-spiral distribution are calculated by

$$\theta_k = \arccos z_k, \ \varphi_k^{(n,q)} = c_{N_S}^{(n)}\theta_k + d\varphi_n^{(q)}. \quad (15)$$

It is convenient to choose an odd number for N_s. In this case, the middle spiral point lays on the equator and a half-spiral ends on the equator.

3. Symmetry of spirals

The spiral described by Eqs. (10)-(15) has C_2 symmetry with respect to the point, at which it crosses equator: $\theta_{(N_s+1)/2} = \pi/2$ and $\varphi^{(n)}_{(N_s+1)/2} = c^{(n)}_{N_S}\pi/2$. Usually, spin systems with the point symmetry group D_n have C_2 axis perpendicular to the C_n axis ($C_2 \| \mathbf{y}$). To use the dihedral symmetry, we must adjust the crossing point to **y**-axis subtracting a constant shift $\varphi^{(n)}_{N_s}$ for all spiral points

$$\varphi^{(n)}_{N_s} = \frac{\pi}{2}\left(4\, round\left(\frac{1}{4}c^{(n)}_{N_S}\right) - c^{(n)}_{N_S} + 1\right). \quad (16)$$

Therefore, the primary spiral is described by

$$\theta_k = \arccos z_k\,,\ \varphi^{(n,0)}_k = c^{(n)}_{N_S}\theta_k - \varphi^{(n)}_{N_s}. \quad (17)$$

Note that the C_2 symmetry of the single spiral distribution does not lead to a decrease of calculation time, as for arbitrary k-th direction the resonance fields $B_0(k)$ of the upper spiral part and fields $B_0(N_s - k)$ for the symmetrical direction of the lower spiral part are different in general case.

In the bispiral approach a second spiral, which is shifted on the azimuthal angle $d\varphi$ with respect to the first primary spiral, is used. For the second spiral

$$\theta_k = \arccos z_k\,,\ \varphi^{(n,1)}_k = c^{(n)}_{N_S}\theta_k - \varphi^{(n)}_{N_s} + d\varphi. \quad (18)$$

If a spin system has a symmetry axis of n-th order, the resonance fields for all points of the second spiral shifted by $d\varphi = d\varphi^{(1)}_n$ are identical to the fields of the primary spiral. We shall denote such spirals as equivalent ones (Fig. 4).

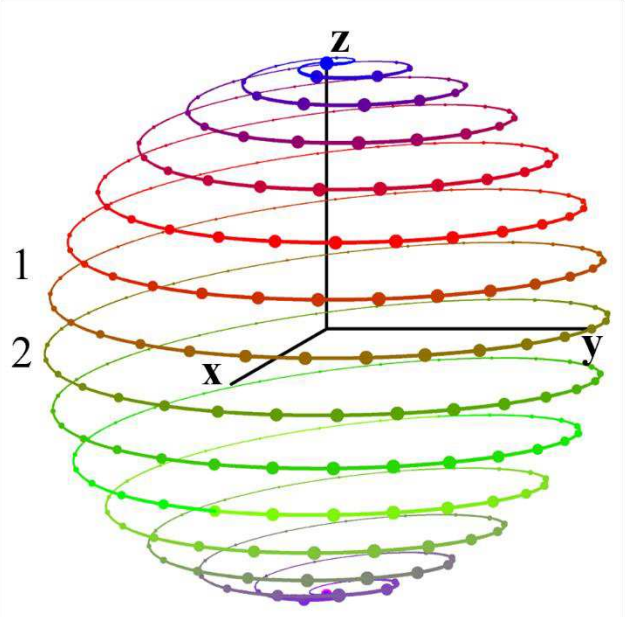

Figure 4. (**Color online**) Reference directions (large circles) and spiral points for two equivalent spirals (1 and 2) of a bispiral for C_2 point group symmetry, $d\varphi = 180^o$, N_s=135. The coloration of reference points and spiral lines reflects the fact that resonance magnetic fields are changed along spirals.

A family of n equivalent spirals has D_n symmetry. The $\theta\varphi$ space between the first and the second spirals of the family is sufficient for spectrum simulations of centers with D_n symmetry: $A_S = 4\pi/n$. To avoid repetitive contributions of equivalent spiral points to the sum (1), the weight factor for both spirals are chosen as $w_k(1) = w_k(2) = 0.5$. Only one of the North or South Poles should contribute to the sum (1) for both spirals.

4. Interpolation

It is possible to join neighbor points of two spirals with a triangular net, and to use corresponding values of $B_0(k)$ on these two spirals as reference points for an interpolation of resonance fields along spirals, and the most important, between the spirals. The triangular partitioning of the space between two spirals allows to implement both spectral smoothing approaches: sub-partitioning and tent.

The simplest way to implement bispiral approach for spin systems with C_1 symmetry is to draw the second equivalent spiral with the shift $d\varphi = 360^o$. In this case, points of the secondary spiral coincide with the points of the primary spirals. The $\theta\varphi$ space between these two spirals is the sphere (Fig. 1, BS).

Another choice for the C_1 symmetry is to draw an independent spiral with the shift $d\varphi = 180^o$ (Fig. 5). In general, resonance fields for such a second spiral are not equal to ones of the primary spiral (we shall denote such a spiral as a complementary one). The N reference points

are shared between primary and complementary spirals: $N_s{=}N/2$, and $w_k(1){=}\ w_k(2){=}1$. The $\theta\varphi$ space between these two spirals is exactly equivalent to the hemisphere.

The sub-partition scheme [45] supposes a division of a reference triangle into smaller triangles and finding interpolated resonance fields in the vertices of the small triangles. The simplest way to get the interpolation directions for bispiral triangles is the recurrent dichotomy of the corresponding θ and φ angles or arcs for the primary triangles. In this case, the total number of directions in a triangle is equal to $(2^{q-1}+1)\ (2^q+1)$, where q is the dichotomy step number. For q equal to 1, 2, 3, 4, and 5 the total numbers are 6, 15, 45, 153, and 561. The first and the last values are not very useful.

For regular axial grids with equilateral triangles (Fig. 1, A), two of three vertices of reference triangles have the same θ_k; therefore, many points inside the triangles have the same $\theta_{km} = \theta_k + m(\theta_{k+1} - \theta_k)/N_p, m = 0, \dots, N_p$ (N_p – number of layers in the sub-partition), but different values of $\varphi_{kmj}, j = 0, \dots, m$. The discreteness has no influence on calculated spectra of centers with strong azimuthal anisotropy, but causes jugging (banding) of spectra of axial and nearly axial centers for axial distribution. In the case of two spirals (Fig. 5), all vertices of inclined triangles have different θ_k and φ_k, producing different θ and φ for every point in the sub-partition (green dots in Figs. 5 and 6). For axial centers, the bispiral and random distributions produce N different θ directions, whereas regular axial grids produce only about $\sqrt{N}$ directions.

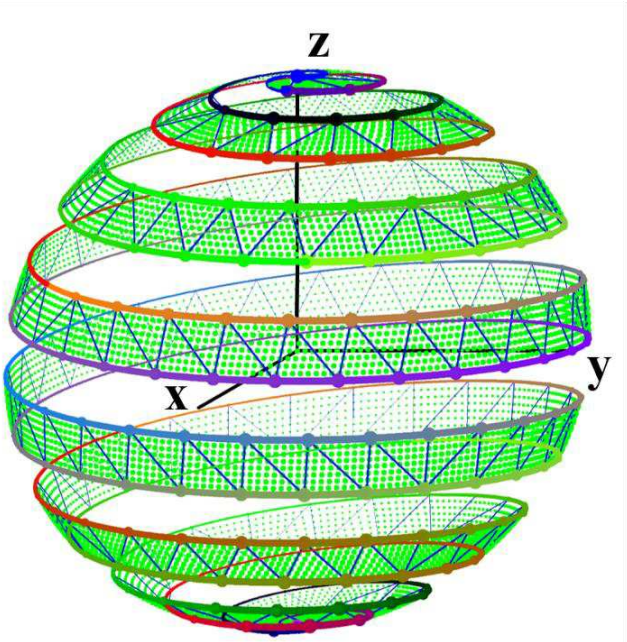

Figure 5. (**Color online**) Reference directions (large circles) and triangles for primary and complementary spirals of the bispiral partition at N_s=135 for C_1 point group symmetry. Green dots are interpolation directions for $N_{i,w}$=32. The spirals colors reflect the fact that resonance magnetic fields for primary and complementary spirals are independently changed along the spirals.

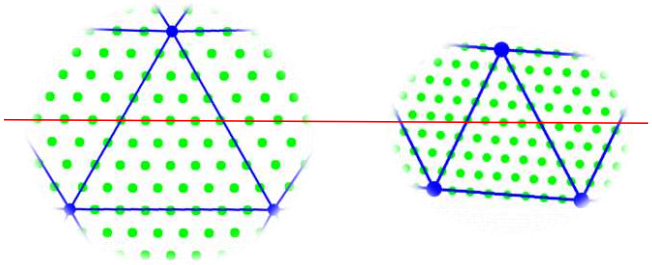

Figure 6. (**Color online**) Sub-partitions with $N_{i,w}$=32 additional directions (green dots) for axial (left) and bispiral (right) distributions. Red line is a parallel of a constant θ.

To avoid repeated summation over equivalent points, the weight w_k should be different for vertex, edge and inner face points. For equivalent spirals

$$w_k = \begin{cases} 1/6 & \text{vertex points} \\ 1/2 & \text{edge points} \\ 1 & \text{face points} \end{cases} \tag{19}$$

Therefore, the total number of points used for the calculation of interpolated spectra is

$$N = N_{tr} N_{i,w} \tag{20}$$

$$N_{i,w} = \frac{N_v}{6} + \frac{N_e}{2} + N_f, \tag{21}$$

where N_v, N_e, and N_f are numbers of vertices, points on edges and face points for a reference triangle ($N_v = 3$). For q equal to 1, 2, 3, 4, and 5 the $N_{i,w}$ are 2, 8, 32, 128, and 512. The number of triangles N_{tr} depends on the partition scheme and the number of reference directions: $N_{tr} \approx 2N_{ref}$ for a very large N_{ref} (Fig. 7).

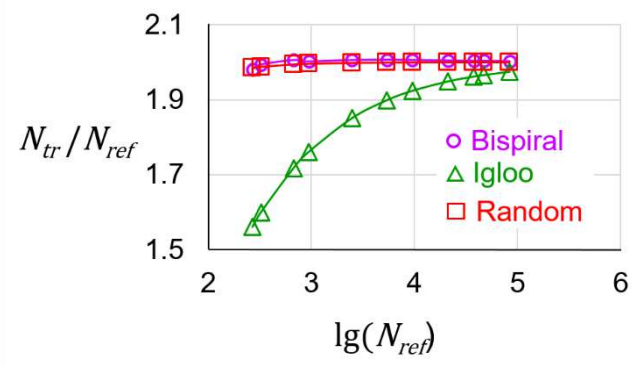

Figure 7. (**Color online**) Dependence of the number of triangles on the number of reference directions.

Comparison of Figs. 2, 3 (calculated with $N = N_{ref}$≈21184, N_i=0) and Figs. 8, 9, 10 (calculated for the same $\theta\varphi$ space for C_1 symmetry with smaller N_{ref}≈5420, but with $N_{i,w}$=32 or tent smoothing) shows that the triangulation, sub-partitioning and interpolation expressively improves the spectrum quality of all partition schemes. However, a non-removed jugging is still observed on the A-spectrum for nearly axial g-tensor (Fig.9, A) due to the reason described above. The jugging is more pronounced if first derivatives of absorption spectra are calculated.

The cause of the visible jugging on R-spectra (Fig. 8, 9, and 10) is that triangles for random distributions have very different sizes. The resonance field interpolation for the largest triangles is less accurate than for the smallest ones and sometimes can even fail. If the interpolation procedure is used with N_{ref}≈5420 and $N_{i,w}$=32, the R-spectrum is worse than A- and BS-spectra for the case of comparable values of g_{20} and g_{22} (Fig. 8). The A-spectrum is worse than bispiral spectra for the nearly axial g-tensor with $g_{20} >> g_{22}$ (Fig. 9 and 10). The tent interpolation (Fig. 10) and the average over additional directions produces comparable spectra.

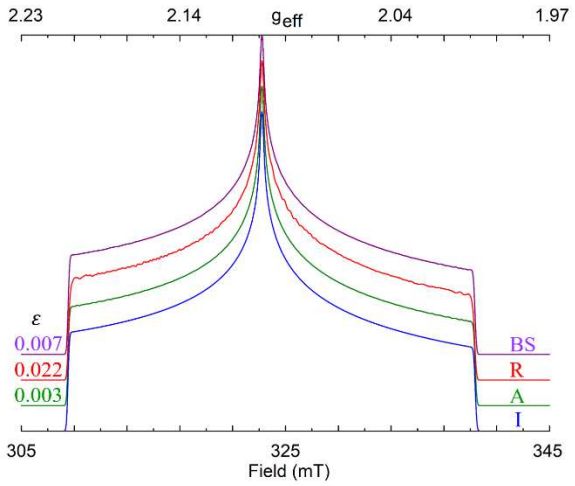

Figure 8. (**Color online**) Simulated spectra for Igloo (A, N_{ref} =5420), random (R) and bispiral (BS) distributions (N_{ref}=5421) at $N_{i,w}$=32 for all partitions; g_{xx}=2.0, g_{yy}=2.1, g_{zz}=2.2, W=0.2 mT. I is the ideal spectrum.

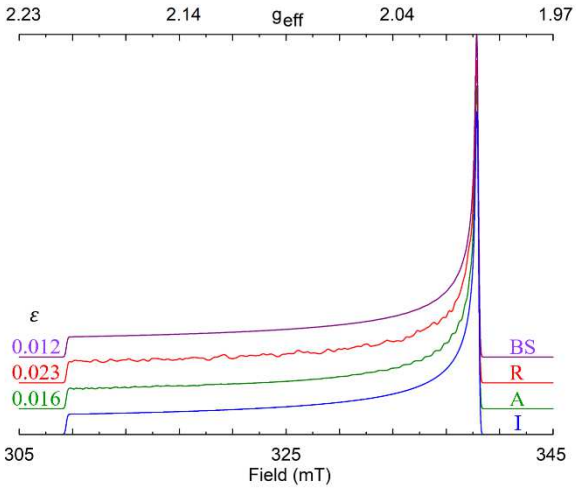

Figure 9. (**Color online**) Simulated spectra for Igloo (A, N_{ref}=5420), random (R) and bispiral (BS) distributions (N_{ref} =5421) at $N_{i,w}$=32 for all partitions; g_{xx}=2.0, g_{yy}=2.0001, g_{zz}=2.2, W=0.2 mT. I is the ideal spectrum. Right peaks were brought together for the ε evaluation.

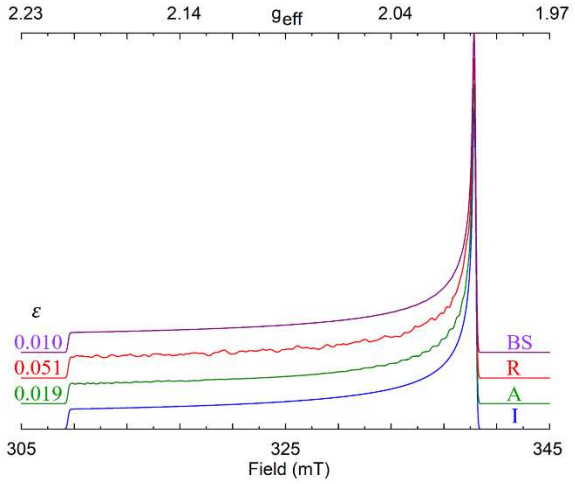

Figure 10. (**Color online**) Simulated spectra for Igloo (A, N_{ref} =5420), random (R) and bispiral (BS) distributions (N_{ref} =5421) smoothed with the tent for all partitions; g_{xx}=2.0, g_{yy}=2.0001, g_{zz}=2.2, W=0.2 mT. I is the ideal spectrum. Right peaks were brought together for the ε evaluation.

5. Spin system symmetry and reduction of the θφ space

Symmetry properties for a specific magnetic system allow a reduction of required $\theta\varphi$ space increasing the point density d for a given number of reference directions N_{ref} used for spectrum calculation [2, 9]. The smaller the $\theta\varphi$ space the smoother are the spectra calculated at the same N_{ref}, i.e. the better is the calculated spectrum quality.

If a paramagnetic center has C_2 symmetry ($C_2\|\mathbf{z}$) then points for a left half of the hemisphere give exactly the same contribution in the sum (1) as points of the right half, i.e. the

N_{ref} points can be distributed over a smaller area giving $d = 2d_h$. For an axial distribution, it is possible to draw a reference meridian, 1 (for instance, at φ=0°) and an equivalent meridian, 2 (at φ=180°).

For a symmetry with an additional vertical mirror plane (like C_{2v}), an additional meridian in the middle between the reference and equivalent meridians (at φ=90°) separates two equivalent $\theta\varphi$ areas. In this case, the N points are distributed over the space between the equator, reference, and middle meridians, i.e. over one quarter of the hemisphere, giving $d = 4d_h$. As the reference and middle (complementary) meridians are independent, $w_k(1) = w_k(2) = 1$. The reference, equivalent, and complementary meridians for centers with C_2, C_3, C_4, and C_6 axes and corresponding minimal $\theta\varphi$ spaces are shown on Fig. 11. To obtain minimal sectors for T, T_h, O_h, O and T_d cubic symmetry groups, additional restrictions are introduced on both θ and φ angles [9].

As for random partitions the meridians do not coincide with boundaries of triangles, such a reduction does not increase spectrum quality: some random prongs may appear in the interpolated R-spectra.

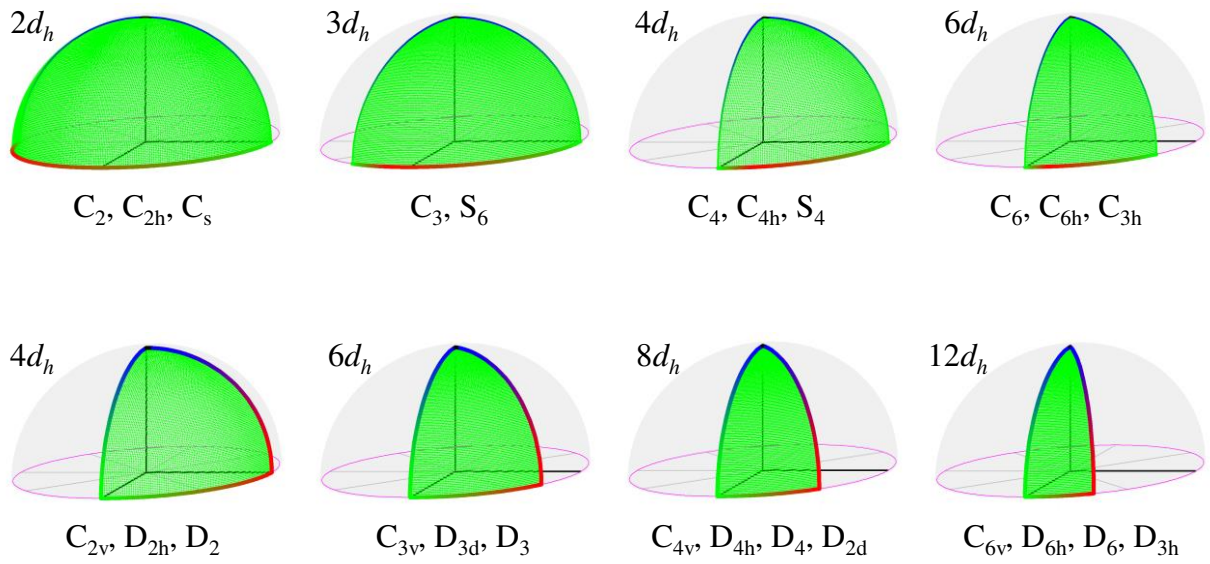

Figure 11. (**Color online**) Minimal sectors and corresponding point densities for groups with C_2, C_3, C_4, and C_6 symmetry axes for axial and random partitions. Thick and thin boundary lines correspond to the weights w_k, which are equal to 1 and 0.5. The equivalent and independent complementary meridians have different colorations that reflect possible different changes of resonance magnetic fields along the meridians.

Bispiral approach allows significant increase of the point density d for paramagnetic centers with symmetry higher than C_1 by a proper choice of the relative positions of the primary reference spiral and equivalent or complementary second spirals described below.

For dihedral symmetries with $C_2\|\mathbf{y}$, the number of the resonance fields B_0 calculated for nonequivalent points on the spirals 1 and 2 halved because

$$B_0(1, N_s - k) = B_0(1, k). \quad (22)$$

$$B_0(2, N_s - k) = B_0(2, k). \quad (23)$$

If used spin-Hamiltonian is written for $C_2\|\mathbf{z}$, then due to symmetry of this spin-Hamiltonian the spiral 2 can be chosen with the shift $d\varphi$=180° (equivalent spiral). For the equivalent spiral 2 the following relation exists

$$B_0(2, k) = B_0(1, k), \quad (24)$$

In both cases, there are only N_s independent reference points and the effective density d for used $\theta\varphi$ space is doubled.

If considered spin system has C_n symmetry with n=3, 4, 6 ($C_n\|\mathbf{z}$), the equivalent spirals are drawn with the shift $d\varphi$ equal to 120°, 90°, and 60°, correspondingly. The equivalent spirals have identical B_0 for the same θ_k, but $\varphi_k \rightarrow \varphi_k + d\varphi$; i.e. the two spirals have $N_s = N_{ref}$ independent reference points. It is similar to the reduction of the hemisphere to the 120°,90°, and 60° sectors for C_3, C_4, and C_6 symmetry for axial distributions (Fig. 11).

For centers with vertical mirror planes, a second independent (complementary) spiral 2 is built in the middle between two equivalent spirals. For instance, two equivalent spirals for C_{2v} symmetry (said 1 and 3) are shifted by 180°; the spiral 2 is built with a shift $d\varphi$=90°. The N_{ref} reference points are shared between the spirals 1 and 2. The triangulation of the $\theta\varphi$ space between spirals 1 and 2 can be used for interpolation. The $\theta\varphi$ space between spirals 2 and 3 gives the same data as for the spiral 1 and 2.

Resonance magnetic fields for the primary spiral 1 and the complementary spiral 2 are different. Therefore, the weight factors w_k for all reference vertices and interpolated points on both spirals as well as for inner face points are equal to 1, whereas $w_k = 1/2$ for edge points. As for the D_n point symmetry groups the upper and lower parts of the $\theta\varphi$ space give identical contributions to the sum (1), half-spirals are sufficient for spectrum simulation. An alternative choice for systems with D_n symmetry is to reuse resonance fields of two equivalent dihedral spirals with $d\varphi = 2\pi/n$ and $w_k(1) = w_k(2) = 0.5$.

It is not clear how to get the minimal $\theta\varphi$ space for cubic symmetry groups using spirals. However, the expected space is only a few percent smaller than the $\theta\varphi$ space for D_2 and C_{4v} groups. The two-dimensional interpolation used in bispiral approach gives a significant spectrum smoothening even for non-minimal $\theta\varphi$ space.

For axial centers with the point symmetry group $D_{\infty h}$, one semi-spiral gives $N = N_s/2$ reference points along the center axis. To use the advantage of two-dimensional interpolation over triangles, two equivalent spiral can be built with an arbitrary small shift $d\varphi$ (said 2-5°).

Fig. 12 and Table 1 summarize properties of two spirals for non-cubic point symmetry groups.

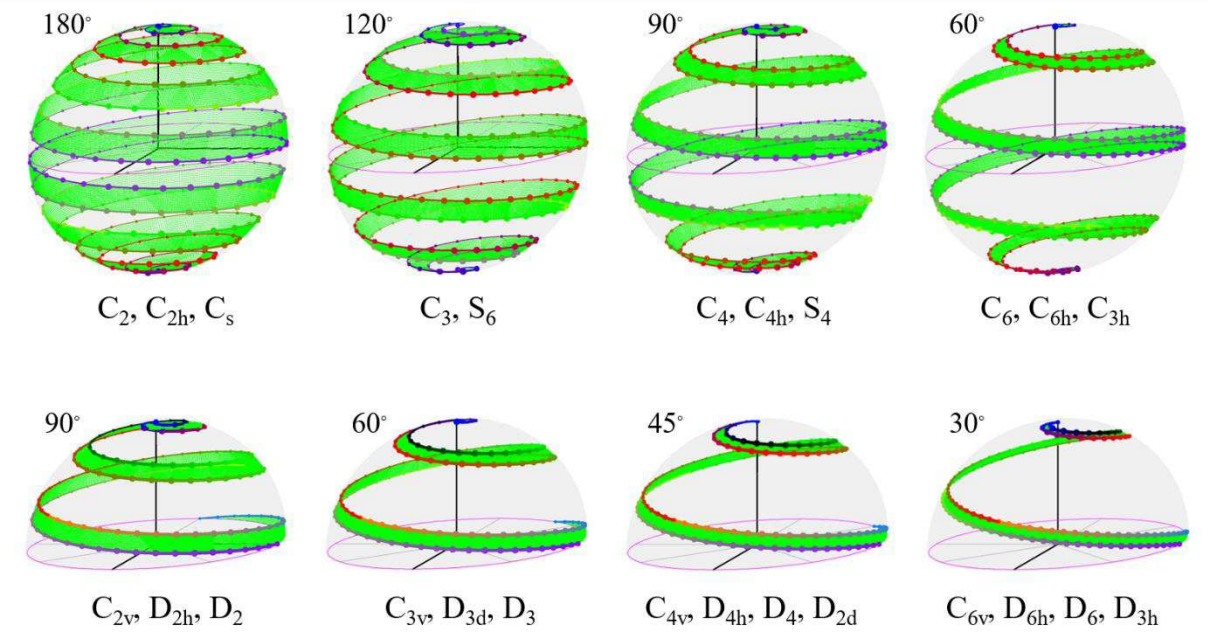

Figure 12. (**Color online**) Bispiral partitions at N_s=135 and $N_{i,w}$ =128. Thick and thin boundary spiral lines correspond to the weights w_k, which are equal to 1 and 0.5. The equivalent and complementary spirals have different colorations. Resonance magnetic fields are changed along spirals in different ways: for the same θ values, they are identical for primary and equivalent spirals, but different for primary and independent complementary spirals. The $d\varphi$ shift between spirals indicated in the right upper corner.

Table 1. Properties of two spirals for all point symmetry groups.

Point symmetry group of a center	Type of both spirals	$d\varphi$ shift (deg)	Weights w_k for points on both spirals	Area of the $\theta\varphi$ space	Density d
C_1, C_i	Equivalent, reusable Complementary	360 180	0.5 1	4π 2π	d_h
C_2, C_{2h}, C_s (D_1)	Equivalent, reusable	180	0.5	2π	$2d_h$
C_3, S_6	Equivalent, reusable	120	0.5	$2\pi/3$	$3d_h$
C_4, C_{4h}, S_4	Equivalent, reusable	90	0.5	π	$4d_h$
C_6, C_{6h}, C_{3h}	Equivalent, reusable	60	0.5	$\pi/3$	$6d_h$
C_{2v}, D_{2h}, D_2, T, T_d	Equivalent, dihedral, reusable Complementary, dihedral	180 90	0.5 1	π $\pi/2$	$4d_h$
C_{3v}, D_{3d}, D_3	Equivalent, dihedral, reusable Complementary, dihedral	120 60	0.5 1	$2\pi/3$ $\pi/3$	$6d_h$
C_{4v}, D_{4h}, D_4, D_{2d}, O, T_d, O_h	Equivalent, dihedral, reusable Complementary, dihedral	90 45	0.5 1	$\pi/2$ $\pi/4$	$8d_h$
C_{6v}, D_{6h}, D_6, D_{3h}	Equivalent, dihedral, reusable Complementary, dihedral	60 30	0.5 1	$\pi/3$ $\pi/6$	$12d_h$

6. Discussion

Strictly speaking, the observed jugging is a product of interference of distribution point discreteness and periodic spectral set of values for the field/frequency sweep. The right choice for the spectrum resolution is $M >> 5 \div 10\, \Delta B/W$. The optimal N value also depends on the line width W.

It follows from Eqs. (2) and (20) that if the interpolation with additional directions in triangles is used then

$$d = \frac{N_{tr} N_{i,w}}{A_s} \approx \frac{2N_{ref} N_{i,w}}{A_s}. \tag{25}$$

The density d is a general characteristic for all methods. The same d value and correspondingly the same $\varepsilon(d)$ value can be obtained at $N_{ref} = N_0$, and $N_{i,w} = 1$, $A_s = 2\pi$ (all

methods without interpolations, including single spiral approach) or at much smaller value of the $N_{ref} = N_0 A_S / N_{i,w}$ for the same N_0 (methods with unlimited $N_{i,w}$ for triangular interpolations; A_s=2π/3÷ π/6 for axial and bispiral schemes and high-symmetry centers). It means that the proposed triangulation and subsequent interpolation for bispiral and random distributions is capable of producing smooth spectra on a par with the interpolation used for axial distributions [16, 17, 45]. The smoothing via interpolations is useful, when an increase of the N_{ref} is difficult due to restrictions of computer memory or available time. It follows from Eqs. (25) that the use of methods with interpolations can theoretically reduce a total calculation time up to hundred times in comparison with methods without interpolations, if an applied interpolation procedure is significantly faster than calculations for reference points. The values of the time reduction depend on a partition scheme, spin system, line width, and spectral resolution.

To estimate real calculation times, a spectrum S_0 at N_{ref}=93001 for the spiral method (τ_0 is its calculation time) and a set of spectra at N_{ref}=5000÷40000 and $N_{i,w}$=32 (spectra for the bispiral approach) were compared with the reference spectrum obtained at $N \approx 10^7$. The spectrum S_1 with the ε value similar to the value for the S_0 spectrum was selected from the set (τ_1 is its calculation time). The following parameters were used: g_{xx}=2.0, g_{yy}=2.1, g_{zz}=2.2, and W=0.2mT for the spin ½; g=2.0, zero-field splitting parameters b_2^0 =0.4, b_2^2=0.02 cm^{-1}, and W=2mT for spins 3/2, 5/2, and 7/2 (see [46] for notations).

Four dominant contributions to the calculation time were monitored: time for calculation of reference directions and triangulation, τ_t; diagonalization time for spin-Hamiltonian matrices, τ_d; time of interpolation over triangles, τ_i; and time of a conversion of a powder-gram into a spectrum, τ_F, i.e. time of a replacement of one bit stick resonance fields with a line shape function (Eqs. 1 and 3).

Calculation of reference directions, triangle vertices, and interpolation directions takes negligibly minor time for the axial and bispiral distributions due to simple recurrent expressions for them. The time for Delaunay triangulation can reach dozens of seconds for random distributions with a large N_{ref}. Therefore, it is useful to make the triangulation for several N_{ref} values in advance, to save its results to files, and to read these files before every spectrum calculation. This considerably reduces τ_t.

It was found that $\tau_i \ll \tau_d, \tau_F$. The τ_d increases approximately as the cube of the spin-Hamiltonian rank R (however, the time depends on the ratio of Zeeman energy, hyperfine interactions, and zero-field splitting parameters), and is proportional to N_{ref}. The τ_F is proportional to the total number of directions, N, and to the number of resonance transitions at each direction.

The obtained ratio τ_0/τ_1 is about 0.5-0.7 for the spin ½ ($R = 2$). Since the time τ_d for the diagonalization of 2×2 matrices can be less than τ_i and τ_F, calculations with sub-partitions have

no advantage in comparison with straightforward diagonalization of spin-Hamiltonian for all N_{ref} directions of a single spiral. However, τ_d grows, if small hyperfine interactions or zero-field splitting are added to the spin-Hamiltonian as perturbations. Depending on the number of nuclei interacting with the electron, the τ_d growth can increase the τ_0/τ_1 value to values close to 1. The case with the spin ½ is very useful for comparison of different partitions.

For spins 3/2, 5/2, and 7/2 ($R = 4, 6, 8$), the ratios τ_0/τ_1 are approximately equal to 3, 7, and 16, correspondingly. The fast increase of the τ_0/τ_1 ratio for $R > 2$ was expected, since the diagonalization time τ_d rises as R^3, whereas τ_i and τ_F are proportional to the R, if allowed resonance transitions are only taken into account. It means that the large spin and multi-spin systems with high ranks of spin-Hamiltonian (like Fe^{3+} with R=6 or Mn^{2+} with R =36) are favorable ones for bispiral approach applications. The τ_0/τ_1 ratios can be smaller for broad resonance lines.

The τ_F for tent interpolation is comparable with τ_F for the average over sub-partitions. For tent interpolated spectra at M=8192 points the ratios τ_0/τ_1 are 2, 6, and 15 for the ranks $R = 4, 6,$ and 8. However, the tent interpolation is several times slower than the average over additional directions for high-resolution spectra.

To compare real calculation times for different $\theta\varphi$ spaces, a mock center with the C_{6v} symmetry, spin 7/2, and parameters b_2^0 =0.4, b_6^6=0.01 cm^{-1}, W=2mT was used. A spectrum S_0 at N_{ref}=93001 for the spiral method (τ_0 is its calculation time) was compared with the reference spectrum obtained at $N \approx 10^7$. The spectra S_2, S_3, and S_6 with the ε value similar to the value for the S_0 spectrum were selected from the sets of the bispiral spectra for C_2, C_3, and C_6 symmetries at $N_{i,w}$=32 and N_{ref}=2000÷20000 (τ_2, τ_3, and τ_6 are their calculation times). It was found that $\tau_0/\tau_2 \approx 5$, $\tau_0/\tau_3 \approx 15$, and $\tau_0/\tau_6 \approx 35$.

The possibility of the calculation time reduction is important for determination of spin-Hamiltonian parameters by experimental spectrum fitting. Such a fitting demands calculations of at least $(3 \div 4)^v$ spectra per iteration, where v is the number of variable parameters. Calculations for three x-values are required for a localization of a minimum of a one-dimensional function $f(x)$, and the fourth calculation is used to obtain the value of the function in the minimum. The simulation of thousands of spectra is required for $v \geq 5$.

One can say that a special program with a summation of points with smaller steps $\Delta\theta = \pi/N$ distributed over a meridian is sufficient for centers with $D_{\infty h}$ symmetry, as the integral over φ in $S(B)$ is equal to 2π. That is right. However, a small off-axis distortion (like $g_{22} \neq 0$, non-axial hyperfine interaction or non-axial zero field splitting) decreases the center symmetry, and general distributions (Figs. 1, 6, 11, and 12) must be used. For all spin systems with $dB/d\theta >> dB/d\varphi$ and $dB/d\varphi \neq 0$ (or $dv/d\theta >> dv/d\varphi$ and $dv/d\varphi \neq 0$) the bispiral approach is more efficient than algorithms based on axial or random distributions (see Figs. 9 and 10), especially, for magnetic

resonances with small line widths (NMR, EPR of radicals or impurities in very pure, non-defect crystals).

There are numerous examples of systems with weak azimuthal anisotropy [46, 47, 48, 49]. Most paramagnetic centers in cubic, hexagonal, tetragonal or trigonal crystals have point symmetry C_3 or higher. Internal disorder due to nonstoichiometry, intrinsic or extrinsic non-paramagnetic defects decreases their symmetry. Comparison of simulated and measured powder spectra allows estimating the extent of the disorder. The diamond samples with axial C-NV centers are used as a probe of external stresses, electric or magnetic fields; these stresses and fields are small off-axial distortions. Hydrogen and carbon nuclei in organic molecules and radicals often have axes of hyperfine interactions, which do not coincide with the axes of axial g-tensors, and are small off-axial perturbations. There are also many similar examples of nuclear systems studied by NMR.

Comparison of features of different distributions of points on a sphere (Table 2) can help to choose the partition scheme, which is the most suitable for a definite spin system.

Table 2. Features of different distributions of points on a sphere.

Distribution **Feature**	**Axial**	**Random**	**Semi-spiral**	**Bispiral**
Triangulation time	Small	Large	Not applicable	Small
Efficiency for nearly axial and axial centers	Bad	Good	Very good	Very good
Number of additional directions for interpolation	Unlimited	Unlimi-ted *)	<10	Unlimited
Interpolation with tent	Yes	Yes *)	Not applicable	Yes
Calculation time reduction for spin-Hamiltonian matrices of 2, 4, 6, 8 ranks due to interpolation	0.5, 2, 6, 15	0.5, 2, 6, 15	5, 5, 5, 5.6 at N_i=5	0.5, 2, 6, 15
Calculation time reduction for spin 7/2 and spin system symmetry C_2, C_3, and C_6	5, 15, 35	Not applicable	Not applicable	5, 15, 35

*) Interpolation may fail, if very large triangles are accidentally generated.

The bispiral partitioning with the fast triangulation of neighbor points (Fig. 1, BS) can be easily applied for polar vectors and star catalogs [42].

7. Conclusions

The axial distributions have equidistant layers with many different azimuthal points for every layer with a given θ. Therefore, spectra of axial and nearly axial spin systems obtained by a summation over points of axial grids are usually jugged even after an interpolation over additional directions. Spiral grids have a more homogeneous distribution of $\theta\varphi$ values producing smoother spectra at the same number of reference directions.

The independently introduced spiral grids [31, 32, 33, 40, 41, 42, 43, 44] are differently formulated variants of the same unique spiral distribution. The condition (16) allows convenient fixing the point where the spiral crosses the equator, uniting the C_2 symmetry axis of the spiral with the crystalline dihedral axis. The family of n equivalent spirals has D_n symmetry. The first two spirals of the family are used in the bispiral approach.

For spin systems with C_1 symmetry there are two possibilities. The first one is to use two equivalent spirals shifted by $d\varphi = 360^{\circ}$. Points of the secondary spiral coincide with the points of the primary spirals, the $\theta\varphi$ space between these two spirals is the sphere, and the reference points are reused. The second one is to build the primary and complementary spirals shifted by $d\varphi = 180^{\circ}$. In this case, the $\theta\varphi$ space is exactly equal to the phase space of magnetic fields, a hemisphere, and the reference points are shared between two spirals. For systems with C_2 or higher symmetry, the $\theta\varphi$ space is significantly reduced by a proper choice of the φ-shift for the second equivalent or complementary spiral, on a par with the space reduction for axial distributions. Symmetry considerations allow to increase the distribution density improving spectrum quality or to reduce the number of reference directions required for powder spectrum calculations decreasing calculation time.

The space between two spirals is conveniently partitioned by a triangular net. This allows using points on the two spirals as reference points for an interpolation of resonance magnetic fields (or frequencies), by means of sub-partitioning or a tent between resonance fields corresponding to triangle vertices. The triangulation and subsequent interpolation expressively improves all simulated spectra. The tent interpolation and the average over additional directions are able to produce similarly smoothed spectra. However, the tent procedure requires several fold more time for high-resolution spectra with the narrow seed line width.

The bispiral approach is a universal method, as it is equally efficient for any system. For spin systems with comparable polar and azimuthal anisotropies it gives the same results as methods with an axial distribution of points on a sphere; however, it provides smoother spectra for axial and nearly axial systems. In comparison with the single spiral grid, the bispiral approach with interpolations over triangles offers many-fold reduction of the calculation time for large spin or multi-spin systems with high ranks of the spin-Hamiltonian, as well as for systems with C_2 or higher symmetry.

[1] F. K. Kneubühl. Line shapes of electron paramagnetic resonance signals produced by powders, glasses, and viscous liquids, *J. Chem. Phys*. **33**, 1074-1078 (1960). doi: 10.1063/1.1731336
[2] G. van Veen. Simulation and Analysis of EPR Spectra of Paramagnetic Ions in Powders. *J. Magn. Reson.*, **30**, 91-109 (1978). doi.org/10.1016/0022-2364(78)90228-7
[3] Y. G. Kliava. EPR spectroscopy of disordered solids. (Zinante, Riga, 1988.
[4] M. She, X. Chen, X.-S. Yu. A method for evaluation of Hamiltonian and line shape parameters from electron paramagnetic resonance powder spectra. *Can. J. Chem.* **67**, 88-92 (1989). doi.org/10.1139/v89-015
[5] M. Eden and M. H. Levitt. Computation of orientational averages in solid-state NMR by gaussian spherical quadrature. *J. Magn. Reson.* **132**, 220–239 (1998). doi.org/10.1006/jmre.1998.1427
[6] M. J. Duer. Solid state NMR spectroscopy: principles and applications. (John Wiley & Sons, 2008).
[7] M. Eden. Computer simulations in solid-state NMR. III. Powder averaging. *Conc. Magn. Res*. **18A**, 24–55 (2003). doi.org/10.1002/cmr.a.10065
[8] A. Ponti. Simulation of magnetic resonance static powder lineshapes: a quantitative assessment of spherical codes. *J. Magn. Reson.* **138**, 288-297 (1999). doi.org/10.1006/jmre.1999.1758
[9] S. Stoll. Spectral Simulations in solid-State Electron Paramagnetic Resonance. PhD thesis, ETH Zurich, 2003, pp. 1-141. doi.org/10.3929/ethz-a-004529758
[10] S. Stoll. Computational Modeling and Least-Squares Fitting of EPR Spectra. In "Multifrequency electron paramagnetic resonance" (Wiley, 2014), pp. 69-138.
[11] J. R. Pilbrow. Transition Ion Electron Paramagnetic Resonance. (Clarendon Press, Oxford, 1990).
[12] C. Craciun. Homogeneity and EPR metrics for assessment of regular grids used in CW EPR powder simulations. *J. Magn. Reson.* **245**, 63-78 (2014). doi.org/10.1016/j.jmr.2014.05.009
[13] C. Craciun. Behaviour of Twelve Spherical Codes in CW EPR Powder Simulations. Uniformity and EPR Properties. *Studia Ubb Chemia*, LXI, **4**, 177–188 (2016).
[14] R. T. Weber. WIN-EPR SimFonia Manual. (EPR Division, Bruker Instruments, Inc, 1995).
[15] M.J. Nilges. Electron Paramagnetic Resonance Studies of Low Symmetry Nickel(I) and Molybdenum(V) Complexes. PhD thesis, University of Illinois, Urbana, 1979, pp.1-195.
[16] G.R. Hanson, K.E. Gates, C.J. Noble, M. Griffin, A. Mitchell, S. Benson. XSophe-Sophe-XeprView. A computer simulation software suite (v. 1.1.3) for the analysis of continuous wave EPR spectra. *J. Inorg. Biochem*. **98**, 903–916 (2004). doi.org/10.1016/j.jinorgbio.2004.02.003
[17] S. Stoll, A. Schweiger. EasySpin, a comprehensive software package for spectral simulation and analysis in EPR. *J. Magn. Reson.* **178**, 42–55 (2006). doi.org/10.1016/j.jmr.2005.08.013
[18] S. Stoll, A. Schweiger. EasySpin: simulating cw ESR spectra. *Biol. Magn. Reson.* **27**, 299–321 (2007).
[19] V.I. Lebedev. Quadratures on a sphere. *Comput. Math. Math. Phys*. **16**, 10–24 (1976). doi.org/10.1016/0041-5553(76)90100-2
[20] B. Stevensson, M. Eden. Efficient orientational averaging by the extension of Lebedev grids via regularized octahedral symmetry expansion. *J. Magn. Reson.* **181**, 162–176 (2006). doi.org/10.1016/j.jmr.2006.04.008
[21] D. W. Alderman, M. S. Solum, D. M. Grant. Methods for analyzing spectroscopic line shapes. NMR solid powder patterns. *J. Chem. Phys.* **84**, 3717–3725 (1986). doi.org/10.1063/1.450211

[22] A.Kreiter, J.Huettermann. Simultaneous EPR and ENDOR Powder-Spectra Synthesis by Direct Hamiltonian Diagonalization. *J. Magn. Res*on. **93**, 12-26 (1991). doi.org/10.1016/0022-2364(91)90026-P

[23] T. Michaels. Equidistributed icosahedral configurations on the sphere. *Computers & Math. with Applications*, **74**, 605-612 (2017). doi.org/10.1016/j.camwa.2017.04.007.

[24] M. K. Arthur. Point Picking and Distributing on the Disc and Sphere. (ARL-TR-7333, 2015), pp. 1-48. https://apps.dtic.mil/sti/pdfs/ADA626479.pdf

[25] S. Galindo, L. Gonzales-Tovany. Monte Carlo simulation of EPR spectra of polycrystalline samples, *J. Magn. Reson.* **44**, 250–254 (1981). doi.org/10.1016/0022-2364(81)90166-9

[26] H. Niederreiter. Quasi-Monte Carlo methods and pseudo-random numbers. *Bull. Am. Math. Soc.* **84**, 957–1041 (1978). doi.org/10.1090/S0002-9904-1978-14532-7

[27] C. Craciun. Application of the SCVT orientation grid to the simulation of CW EPR powder spectra. *Appl. Magn. Reson*. **38**, 279–293 (2010). doi.org/10.1007/s00723-010-0129-9

[28] M. Bak, N. C. Nielsen. REPULSION, a Novel Approach to Efficient Powder Averaging in Solid-State NMR. *J. Magn. Reson.* **125**, 132–139 (1997). doi.org/10.1006/jmre.1996.1087

[29] I. M. Sobol. Uniformly distributed sequences with an additional uniform property. *U.S.S.R. Comput. Maths. Math. Phys.* **16**, 236–242 (1976). doi.org/10.1016/0041-5553(76)90154-3

[30] I. A. Antonov, V.M. Saleev. An economic method of computing LP_τ-sequences. *U.S.S.R. Comput. Maths. Math. Phys.* **19**, 252–256 (1979). doi.org/10.1016/0041-5553(79)90085-5

[31] M. J. Mombourquette and J. A. Weil. Simulation of Magnetic Resonance Powder Spectra. *J. Magn. Reson.* **99**, 37-44 (1992). doi.org/10.1016/0022-2364(92)90153-X

[32] E.B. Saff, A.B.J. Kuijlaars. Distributing many points on a sphere. *Math. Intell.* **19**, 5–11 (1997).

[33] V. Grachev. Double spiral and fractal approaches for calculations of EPR and NMR spectra in amorphous solids and powders. *Specialized Colloque AMPERE* "ESR and Solid State NMR in High Magnetic Fields", Stuttgart, 2001, p. 50.

[34] R. Swinbank, R.J. Purser. Fibonacci grids: a novel approach to global modelling. *Quart. J. Roy. Meteorol. Soc.* **132**, 1769–1793 (2006). doi.org/10.1256/qj.05.227

[35] N. S. Bakhvalov. On the approximate computation of multiple integrals. *Vestn. Mosk. Univ. Ser. Mat. Meh. Astr. Fiz. Chim.* **4**, 3–18 (1959). doi.org/10.1016/j.jco.2014.12.003

[36] N.M. Korobov. The approximate computation of multiple integrals. *Dokl. Akad. Nauk SSSR,* **124**, 1207–1210 (1959).

[37] A. Gonzales. Measurement of Areas on a Sphere Using Fibonacci and Latitude-Longitude Lattices. *Math. Geosci.* **42**, 49-64 (2010). doi.org/10.1007/s11004-009-9257-x

[38] S. K. Khamas. Moment Method Analysis of an Archimedean Spiral Printed on a Layered Dielectric Sphere. *IEEE Trans. on Antennas and Propagation*. **56**, 345-352 (2008). DOI: 10.1109/TAP.2007.915466

[39] H. Ebert, J. Abart, J. Voitlander. Simulation of quadrupole disturbed NMR field spectra by using perturbation theory and the triangle integration method. *J. Chem. Phys.* **79**, 4719-4723 (1983). doi.org/10.1063/1.445613

[40] C. G. Koay. Analytically exact spiral scheme for generating uniformly distributed points on the unit sphere. *J. Comput. Sci.* **2**, 88–91 (2011). doi.org/10.1016/j.jocs.2010.12.003

[41] S. T. Wong, M. S. Roos. A strategy for sampling on a sphere applied to 3D selective RF pulse design. *Magn. Reson. Med.* **32**, 778–784 (1994). doi.org/10.1002/mrm.1910320614

[42] R. Bauer. Distribution of points on a sphere with application to star catalogs. *J. Guidance, Control, and Dynamics,* **23**, 130–137 (2000). doi.org/10.2514/2.4497

[43] D. P. Hardin, T. Michaels, E. B. Saff. A comparison of Popular Point Configuration on S^2. *Dolomites Research Notes on Approximation*, **9**, 16-49 (2016). arXiv:1607.04590

[44] E. A. Rakhmanov, E. B. Saff, Y. M. Zhou. Minimal discrete energy on the sphere. *Math. Research Letters*, **1**, 647–662 (1994). dx.doi.org/10.4310/MRL.1994.v1.n6.a3

[45] D. Wang, G. R. Hanson. A New Method for Simulating Randomly Oriented Powder Spectra in Magnetic Resonance: The *S*ydney *Op*era *H*ous*e* (SOPHE) Method. *J. Magn. Reson.* **A117**, 1–8 (1995). doi.org/10.1006/jmra.1995.9978

[46] V. G. Grachev, G. I. Malovichko. Structures of Impurity Defects in Lithium Niobate and Tantalate Derived from Electron Paramagnetic and Electron Nuclear Double Resonance Data. *Crystals,* **11**, 339 (2021). doi.org/10.3390/cryst11040339

[47] S. A. Altshuler and B. M. Kozyrev. Electron Paramagnetic Resonance in Compounds of Transition Elements. (Nauka, Moscow, 1972).

[48] F. E. Mabbs, D. Collison. Electron Paramagnetic Resonance of d Transition Metal Compounds. (Elsevier, Amsterdam-London-New York-Tokyo, 1992).

[49] M. V. Vlasova, N. G. Kakazei, A. M. Kalinichenko, A. S. Litovchenko. Radiospectroscopic Properties of Inorganic Materials. A Handbook. (Naukova Dumka, Kiev, 1987).